Space-charge and thermal effects in relativistic crossed-field devices

Samuel Marini, Felipe B. Rizzato, and Renato Pakter

Citation: Physics of Plasmas **25**, 063111 (2018); doi: 10.1063/1.5028384
View online: https://doi.org/10.1063/1.5028384
View Table of Contents: http://aip.scitation.org/toc/php/25/6
Published by the American Institute of Physics

Space-charge and thermal effects in relativistic crossed-field devices

Samuel Marini,[1,2,a)] Felipe B. Rizzato,[1,b)] and Renato Pakter[1,c)]
[1]*Instituto de Física, Universidade Federal do Rio Grande do Sul, Caixa Postal 15051, 91501-970 Porto Alegre, RS, Brazil*
[2]*LULI, Sorbonne Université, CNRS, École Polytechnique, CEA, Université Paris-Saclay, F-75252 Paris cedex 05, France*

(Received 9 March 2018; accepted 28 May 2018; published online 13 June 2018)

In this paper, a fully kinetic theory for the relativistic electron flow in a crossed-field device is developed and analyzed. The theory takes into account self-electric, self-magnetic, and thermal effects and allows determining the final stationary state achieved by the electrons in phase-space. A number of different possible stationary modes are identified and described in detail. Particular attention is given to the study of how space charge and thermal effects affect the magnetic insulation when the external magnetic field exceeds the Hull cutoff field. In the nonrelativistic limit, it is found that there is only a single mode transition that leads to the loss of the magnetic insulation. This transition is completely independent of the electron density and occurs for relatively large injection temperatures. On the other hand, in a moderate relativistic regime a much richer scenario is found with the onset of a series of stationary state mode transitions as both electron density and injection temperature are varied. In particular, it is found that the transitions and the consequent loss of magnetic insulation may occur even at very low injection temperatures. Self-consistent numerical simulation results are also presented and used to verify the theoretical findings. *Published by AIP Publishing.* https://doi.org/10.1063/1.5028384

I. INTRODUCTION

The study and characterization of the dynamics of electrons immersed in a crossed electromagnetic field have attracted a lot of attention over the years due to its relevance in the development of important technological devices such as electric thrusters,[1,2] radars,[3] RF generators,[4] and sputterings.[5] The early models based on single particle dynamics showed that if the magnetic field is strong enough, it can prevent the electrons from reaching the anode.[6] This is the so called magnetic insulation (MI) that occurs whenever the external magnetic field exceeds the Hull cutoff field $B_H = \sqrt{2mV_0/eL^2}$, where m and e are the mass and charge of the electron, and V_0 and L are the cathode-anode voltage difference and distance. This expression is readily obtained if one considers that the electron is emitted from the cathode with vanishing kinetic energy. Nevertheless, it is known since the pioneering works of Child and Langmuir[7,8] that the space charge self-electric field may play a very important role in such non-neutral devices by inducing the onset of a virtual cathode that limits the current density which can be extracted from the cathode.[9] The same effect occurs in crossed field devices.[10] In fact, not only the self-electric field, but also the self-magnetic field may be of relevance.[11,12] This is particularly true when the accelerating potential energy becomes a *sizable* fraction of the electron rest mass and the relativistic effects become noticeable. In this regard, a fully self-consistent theory which includes relativistic effects has been developed for the case of cold injection.[13]

Another important issue that has been investigated is the effect of temperature on the electron injection. It has been shown that thermal velocity spread may affect the magnetic insulation and lead to the onset of stationary states in the space charge limited regime, among other effects.[14–18] However, as a simplifying assumption, all the theoretical investigations done so far that include thermal effects neglect the self-magnetic fields.

In this work, we develop and analyze a fully kinetic theory for the relativistic electron flow in a crossed-field gap that takes into account both self-electromagnetic and thermal effects. The theory allows determining the final stationary state achieved by the electrons in phase-space. We consider that the velocity distribution at injection corresponds to a waterbag distribution and identify four different types of stationary mode solutions. The waterbag distribution is considered not only for its simplicity, but also because it reproduces results from more realistic distributions.[19] Particular attention is given to the study of how space charge and thermal effects affect the magnetic insulation when the external magnetic field exceeds the Hull cutoff field. In the nonrelativistic limit, it is found that there is only a single mode transition that leads to the loss of the magnetic insulation. This transition is completely independent of the electron density and occurs only for relatively large injection temperatures. On the other hand, in a moderate relativistic regime when the self-magnetic fields start to play a role, we find a much richer scenario in the parameter space. A series of stationary state mode transitions that go all the way from complete insulation (when no electrons reach the anode) to no insulation at all (when all the electrons reach the anode) occur as both injection temperature and charge density are varied. In particular, it is found that the transitions occur even at very low injection temperatures. Moreover, two different types

[a)]marini@ufrgs.br
[b)]rizzato@if.ufrgs.br
[c)]pakter@if.ufrgs.br

of non-insulated (NI) stationary states are identified. While on one there is only a single population of electrons where all contribute to the cathode-anode current, on the other there are two distinct electron populations: one that contributes to the cathode-anode current and a more tenuous one that stays trapped in the gap region, not contributing to the cathode-anode current. Such a stationary state is present only when self-magnetic fields and thermal effects are properly taken into account. We also run N-particle self-consistent simulations to verify the theoretical results. A very good agreement is found between the theory and the numerical results.

This paper is organized as follows: in Sec. II, we introduce the theoretical physical model of the relativistic crossed field gap; in Sec. III, we identify and discuss the properties of the different stationary modes obtained from the kinetic theory; in Sec. IV, we investigate based on the theory the changes in magnetic insulation as the parameters are varied; in Sec. V, we present results from the N-particle self-consistent simulations and compare them to the theory; and, finally, in Sec. VI, we draw our conclusions.

II. THEORETICAL MODEL

The geometry and the electromagnetic field configuration of the relativistic crossed-field gap are shown in Fig. 1. There, we can observe two long parallel plates kept at a constant potential difference. The plates are oriented in the xz–plane and separated by a distance L along the y–axis. The plate at $y=0$ is a cathode kept at zero electric potential and the plate at $y=L$ is an anode kept at an electric potential value V_0. As a consequence of the electric potential difference, there is a constant external electric field $\mathbf{E}_0 = -(V_0/L)\hat{\mathbf{y}}$ in the gap between the plates. Moreover, there is a uniform constant external magnetic field $\mathbf{B}_0 = -B_0\hat{\mathbf{z}}$ that is orthogonal to the electric field $\mathbf{E}_0$. This type of electromagnetic field configuration is known as the crossed-field configuration.

At time $t=0$, the cathode starts emitting electrons which enter the gap, being accelerated by the external electric field $\mathbf{E}_0$ along the y–direction and deflected by the external magnetic field $\mathbf{B}_0$ along the clockwise direction. It means that the electrons released by the cathode may not reach the anode because of the magnetic field. Indeed, if the magnetic field is such that $B_0 > B_H$, it can be shown that electrons emitted from the cathode with vanishing velocities will not reach the anode in the non-relativistic regime $eV_0/mc^2 \ll 1$.[6] However, in addition to the influence of the external electromagnetic fields, the electron flow is influenced by the fields self-generated by the electron distribution, such that $\mathbf{E} = \mathbf{E}_0 + \mathbf{E}_s$ and $\mathbf{B} = \mathbf{B}_0 + \mathbf{B}_s$. Hence,

FIG. 1. Geometry and field configuration of a crossed field device. The electrons are emitted by the cathode and their trajectories are determined by the electromagnetic fields inside the gap region which include both externally and self-generated fields.

to properly describe the electron flow behavior when the self-fields and the relativistic effects are non-negligible, we develop a kinetic theory that explicitly takes into account such effects. To start, let us consider the Hamiltonian that describes the dynamics of each particle in the gap

$$H = c\sqrt{m^2c^2 + (\mathbf{P} + e\mathbf{A})^2} - e\phi, \tag{1}$$

where m and e are the mass and the charge of the electron, c is the speed of light in vacuum, $\mathbf{P}$ is the particle canonical momentum, and ϕ and $\mathbf{A}$ are the total electric and vector potentials that take into account both external and self-fields.

Given the symmetry of the cathode and the anode plates, we assume that the electron distribution is uniform along that xz–plane, such that all the field quantities only depend on the y coordinate. From the Poisson equation, we obtain that the electric potential is given by

$$\frac{\partial^2\phi}{\partial y^2} = \frac{e}{\varepsilon_0}n(y), \tag{2}$$

satisfying the boundary conditions $\phi(y=0)=0$ and $\phi(y=L) = V_0$. In Eq. (2), ε_0 is the permittivity of free space and $n = \int f(y,\mathbf{P})d\mathbf{P}$ is the electron density obtained integrating the particle distribution function on the phase space. It is easy to see that when there is no charge inside the gap, Eq. (2) reproduces the external electric field. In a crossed field device, the electrons are not only accelerated along the gap direction by the external electric field but also in a transverse direction due to the external magnetic field. In the configuration considered here, this corresponds to a flow in the x direction which is responsible for the generation of a self-magnetic field that tends to shield the cathode from the external magnetic field. Because the magnetic generated current is along the x direction, the relevant component of the vector potential is A_x which is determined by Ampere's law as given by

$$\frac{\partial^2 A_x}{\partial y^2} = e\mu_0\bar{v}_x(y)n(y), \tag{3}$$

satisfying the boundary conditions $\partial A_x/\partial y|_{y=L} = -B_0$ and $A_x(y=0)=0$, where μ_0 is the permeability of free space and $\bar{v}_x(y)$ is the average (fluid) transverse velocity at position y. These boundary conditions are consistent with a stationary solution where the electromagnetic fields have become time independent in the system.[20,21]

The particle Hamiltonian (1) can then be written as

$$H = c\sqrt{m^2c^2 + [P_x + eA_x(y)]^2 + P_y^2 + P_z^2} - e\phi(y). \tag{4}$$

The Hamiltonian given by Eq. (4) does not explicitly depend on x and z variables; consequently, P_x and P_z are constants of motion and their values are determined by the initial conditions. We assume that the electrons are emitted with vanishing parallel velocities to the cathode plane. It means that $P_x(0) = P_z(0) = 0$ and $P_y(0) = P_0$, where P_0 is the initial momentum of the electron at the cathode which is non-null only along the y direction. We stress that this initial condition does not imply that the velocity parallel to the cathode is

always zero, indeed $\mathbf{v}_{\parallel} = (\mathbf{P}_{\parallel} + e\mathbf{A}_{\parallel})/\sqrt{m^2 + (\mathbf{P} + e\mathbf{A})^2/c^2}$. Therefore, as discussed above, the x component of the velocity is nonvanishing due to the magnetic field and is given by

$$v_x(y, P_y) = \frac{ecA_x}{\sqrt{m^2c^2 + P_y^2 + e^2A_x^2(y)}}. \tag{5}$$

The thermal effects are characterized by a dispersion around the mean momentum. Here, we assume that the momentum dispersion of the electrons entering the gap satisfies a waterbag distribution. Such distribution is considered not only because it is simple, but also because it reproduces results from more realistic distributions.[19] We write the waterbag distribution at emission as

$$f(y = 0, P_y) = n_0 \frac{\Theta(P_y) - \Theta(P_y - P_{0max})}{P_{0max}}, \tag{6}$$

where n_0 is the electron density at the emission and Θ is the Heaviside step function whose value is zero for negative argument and one for positive argument. In Eq. (6), P_{0max} is the momentum of the faster electrons in the distribution and is therefore related to the injection temperature. Note that we assume that the electrons are *not* pre-accelerated before entering the gap region. The slower electrons are thus injected with vanishing velocities. Given the injection distribution function of Eq. (6), we can estimate the mean electron velocity along the gap as given by $\bar{v}_x(y) = (1/P_{0max}) \int_0^{P_{0max}} v_x(y, P_y) dP_y$. Using Eq. (5), we obtain

$$\bar{v}_x = \frac{ecA_x}{\sqrt{m^2c^2 + e^2A_x^2}} \tan^{-1}\left(\frac{P_{0max}}{\sqrt{m^2c^2 + e^2A_x^2}}\right), \tag{7}$$

which can be substituted in Eq. (3). We stress that in our model the electron injection temperature is not isotropic because we only consider thermal effects along the direction transverse to the cathode plane.

III. STATIONARY SOLUTIONS

Once the system has reached the steady state, all variables become time independent. In particular, the single particle Hamiltonian of each electron becomes a conserved quantity. From the energy conservation, $H(y) = H(y = 0)$, we can write the absolute value of the momentum of a given electron as a function of the position as

$$P_y(y, P_0) = \sqrt{P_0^2 - e^2A_x^2 + \frac{e\phi}{c}\left(\frac{e\phi}{c} + 2\sqrt{m^2c^2 + P_0^2}\right)}. \tag{8}$$

Electrons with a positive (negative) momentum are moving towards the anode (cathode). Using Eq. (8) and a method analogous to the one developed in Refs. 16 and 17, which are based on the incompressibility in phase space of the Vlasov equation that dictates the evolution of the electron flow, we can obtain expressions for the stationary electron density as a function of the electromagnetic potentials, i.e., $n(\phi, A_x)$. Substituting this in Eqs. (2) and (3), we then obtain a closed set of equations to determine the stationary solutions. It is worth noting that since the present method is based on the Vlasov equation, it does not take into account collisional effects.[22] We identify that for the relativistic flow considered here there are four different types of modes of stationary electron flow that may appear as the parameters are varied. These different modes and their characteristics are described below.

A first mode is a magnetic insulated (MI) flow where all the electrons emitted from the cathode eventually return to it, such that there is no anode current. This type of stationary solution has been studied in detail in the nonrelativistic regime in Ref. 16. It was shown that although the particles are initially distributed along an *annular* region in phase space bounded by the curves that represent the phase space orbits of the initially slowest and fastest electrons, namely, $P_y(y, 0)$ and $P_y(y, P_{0max})$, when the slowest electrons are injected with vanishing velocities, the inner region ends up being completely filled between $\pm P_y(y, P_{0max})$ due to an instability as it approaches the stationary state. Hence, the electron density as a function of the coordinate can be written as

$$n_{MI}(y) = 2n_0 \frac{P_y(y, P_{0max})}{P_{0max}}, \tag{9}$$

since $2P_y(y, P_{0max})$ is the area occupied by the flow in the phase space. Here, the factor "2" accounts for the fact that the same fraction of electrons that are moving to the anode is moving back to the cathode in this mode [see Fig. 2(a)].

A second mode is a completely noninsulated (NI) flow where all the electrons eventually reach the anode, causing a gap closure. In this stationary configuration, the electron density as a function of the coordinate is given by

$$n_{NI}(y) = n_0 \frac{P_y(y, P_{0max}) - P_y(y, 0)}{P_{0max}}. \tag{10}$$

Since in this case even the slowest electrons reach the anode, the curve $P_y(y, 0)$ plays a role in defining the stationary solution. The area occupied by the particles in the phase space is $P_y(y, P_{0max}) - P_y(y, 0)$ [see Fig. 2(b)].

A third mode is a partially insulated (PI) flow because part of the electrons reach the anode and part, return to the cathode. This mode can be seen as a composition of the two previous ones. The electrons emitted from the cathode with momentum ranging from $P_0 = 0$ and a limiting momentum P_{0lim} return to it after a transient time. The mathematical treatment for these electrons is equal to the MI mode. On the other hand, the electrons with momentum between P_{0lim} and P_{0max} reach the anode. The mathematical treatment of these electrons is equal to the NI mode. Here, P_{0lim} is defined as the minimum momentum required for an electron emitted from the cathode with $P_0 = P_{0lim}$ reach the anode [see Fig. 2(c)]. Clearly, $0 < P_{0lim} < P_{0max}$ must be satisfied. In this case, the electron density becomes

$$n_{PI}(y) = 2n_0 \frac{P_y(y, P_{0lim})}{P_{0max}} + n_0 \frac{P_y(y, P_{0max}) - P_y(y, P_{0lim})}{P_{0max}}. \tag{11}$$

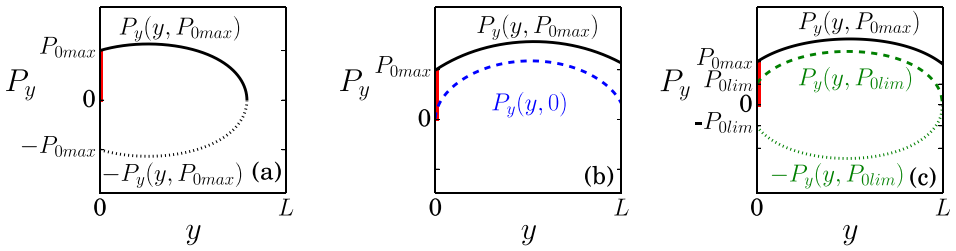

FIG. 2. Representation of the phase space showing the curves that delimit the particle distribution in the different stationary modes. Panel (a) represents the MI mode where the particles do not reach the anode and are distributed between $\pm P_y(y, P_{0max})$. Panel (b) represents the NI mode where all the particles reach the anode and are distributed between $P_y(y, 0)$ and $P_y(y, P_{0max})$. In panel (c), the particles located between $\pm P_y(y, P_{0lim})$ do not reach the anode, whereas those located between $P_y(y, P_{0lim})$ and $P_y(y, P_{0max})$, reach the anode. It serves to describe both PI and NI* modes. While in the PI mode the particles are distributed between $-P_y(y, P_{0lim})$ and $P_y(y, P_{0max})$ with the same density, in the NI* mode, there is a lower density particle distribution between $\pm P_y(y, P_{0lim})$ and a higher density distribution between $P_y(y, P_{0lim})$ and $P_y(y, P_{0max})$.

For some parameters, we notice that a solution of the PI form given by Eq. (11) is found but with a negative P_{0lim}. This solution is nonphysical because the lowest injection velocity possible is zero. However, if, in these cases, we set $P_{0lim} = 0$ and allow the existence of a *tenuous* particle distribution within the phase space region bounded by $-P_y(y, P_{0lim})$ and $+P_y(y, P_{0lim})$ [see Fig. 2(c)], then a new stationary solution is found by the theory. When we say, tenuous, we mean with a density that is lower than the injection density n_0. Note that this lower density distribution does not contradict the incompressibility imposed by the Vlasov equation. In fact, the Vlasov equation only sets a maximum density that can be found in the phase-space – n_0 in this case – but does prevent the occurrence of lower densities in a coarse grained sense.[23,24] In any case, it is worth mentioning that the onset of lower density distributions was not observed in previous nonrelativistic studies[16,17] and is, therefore, a consequence of the relativistic and self-current effects. Since the tenuous distribution is bounded by the $\pm P_y(y, P_{0lim})$ curves in phase space, we notice that these particles are not in contact with neither the cathode nor the anode; they are actually trapped in the gap region and do not contribute to the anode current. On the other hand, all the electrons that are being launched from the cathode with $0 \le P_0 \le P_{0max}$ eventually reach the anode. In this respect, this mode corresponds to a modified noninsulated stationary solution that we refer to as NI*. The corresponding density can be written as

$$n_{NI^*}(y) = n_0 \frac{P_y(y, P_{0max})}{P_{0max}} + n_0(2\delta_{n_0} - 1)\frac{P_y(y, 0)}{P_{0max}}, \tag{12}$$

where $0 \le \delta_{n_0} \le 1$ is the density variation for the trapped particles distribution, which can be self-consistently determined by imposing that the electron emitted with $P_0 = 0$ reaches the anode with zero momentum, i.e., $P_y(y = L, 0) = 0$. This corresponds to a fourth type of stationary solution. It is worth noting that when $\delta_{n_0} = 0$, Eq. (12) reduces to the NI mode given by Eq. (10), whereas when $\delta_{n_0} = 1$, it reduces to the PI mode given by (11).

In practice, in order to determine the stationary solution for a given set of parameters we initially *assume* that the stationary flow belongs to one of the four modes described above and use the corresponding charge density to solve the equations for the electric (2) and vector (3) potentials. Inspecting the trajectories of the most and least energetic electrons for the solution found, we can then validate or discard the initial assumption made about the flow mode. For instance, if we initially assume that the flow is a MI mode, but end up finding that $P_y(y = L, P_{0max}) > 0$ we see that the solution is inconsistent and a different mode must be assumed. In our analysis we find that for a given set of parameters, there is only one consistent stationary solution. The numerical code that we developed automatically tests for the different modes with charge densities given by Eqs. (9)–(12) to determine the fully consistent stationary solution.

IV. MAGNETIC INSULATION ANALYSIS

The main purpose of the present paper is to investigate how the self-fields may change the overall electron flow in relativistic regimes. More specifically, since the magnetic insulation is an important issue in crossed-field devices, we want to determine how it may be affected by the self-fields as the parameters are changed. In order to simplify the analysis, we conveniently normalize the space variable to L and the momentum to eB_0L. We also define the scaled parameters $\nu_0 = 2mV_0/eB_0^2L^2$, $\eta_0 = en_0L^2/\epsilon_0V_0$, $T_0 = P_{0max}^2/12e^2B_0^2L^2$, and $\xi_0 = \mu_0\epsilon_0eV_0/m = eV_0/mc^2$ which measure, respectively, the voltage to magnetic insulation ratio, the charge intensity, the injection temperature, and the normalized potential. These scaled quantities completely characterize the system properties. In the absence of thermal and self-field effects, the insulation is solely determined by the parameter ν_0. In particular, for $\nu_0 < 1$ a single particle ejected from the cathode with vanishing velocity does not have enough energy to reach the anode, guaranteeing the magnetic insulation. With that in mind, for the remainder of the paper we fix $\nu_0 = 0.8$ and investigate how thermal, relativistic, and self-field effects affect the insulation.

In Fig. 3, a parametric plot showing the stationary solution mode found as a function of the normalized charged density η_0 and injection temperature T_0 is presented. In panel (a), the results for a nonrelativistic case with $\xi_0 \to 0$ are shown. We observe that as we increase the injection temperature, the electron flow goes from the MI to the PI mode when $T_0 \approx 0.017$. This occurs because for such *large* injection temperatures there are already some electrons that are

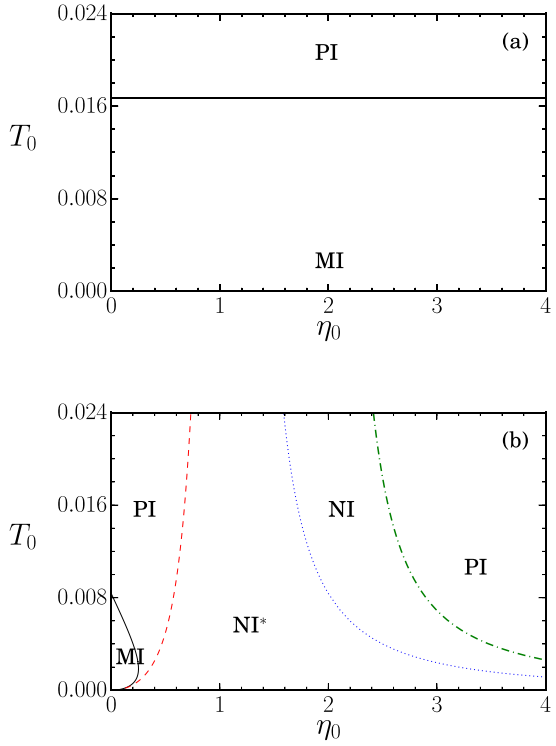

FIG. 3. Parameter space showing the stationary solution mode predicted by the theory as a function of η_0 and T_0. In (a), we consider a nonrelativistic case with a small relativistic parameter $\zeta_0 = 0.0002$. The only transition found is a MI to PI that occurs as the normalized temperature exceeds $T_0 \approx 0.017$. On the other hand, for the moderately relativistic case with $\zeta_0 = 0.2$ shown in (b), it is a found a much richer scenario with many mode transitions appearing as the temperature and charge intensity parameters are varied. The curves represent where the mode transitions occur: MI to PI (black solid curve), PI to NI* (red dashed curve), NI* to NI (blue dotted curve), and NI to PI (green dotted-dashed curve).

launched from the cathode with enough kinetic energy to surpass the magnetic insulation and reach the anode. We also observe that the normalized charge intensity η_0 plays no role in determining the stationary mode. This is in agreement with previous nonrelativistic analysis.[16] In panel (b), we consider a moderately relativistic case with $\xi_0 = 0.2$. This corresponds to an accelerating potential of the order of $V_0 \approx 100$ KV.[25] Now, we find a much richer scenario with many transitions occurring in the electron stationary flow and in the resulting magnetic insulation. In particular, we observe that, differently from the nonrelativistic case, not only injection temperature, but also charge intensity play a major role in determining the stationary mode. This is related to the fact that as relativistic effects become more important, the space charge does not only affect the accelerating electric field but can also generate self-magnetic fields which may change the insulation properties. In particular, it should be noted that in the moderately relativistic case mode transitions and the consequent loss of magnetic insulation occur even at relatively low injection temperatures.

To investigate how the fields are affected by the charge distribution in the relativistic case of Fig. 3(b), we compute the cathode electric and magnetic fields as a function of the normalized charge density η_0 for a fixed injection temperature $T_0 = 0.006$. The results are shown by the curves in Fig. 4. Naturally, when $\eta_0 \to 0$ the space charge effects are negligible and the electromagnetic fields approach the vacuum values $B_c = B_0$ and $E_c = E_0$. However, as the charge intensity is increased the electromagnetic fields at the cathode start to decrease. Because the magnetic insulation is losing its strength, the electron flow tends to get closer to the anode. In particular, when $\eta_0 = 0.16$ the most energetic electrons finally reach the anode and the flow goes from MI (solid line) to PI (dashed line) mode. It is interesting to note that at this transition the cathode magnetic field is just 4% lower than the vacuum field. So, despite being a small variation, it is enough to destroy the magnetic insulation. As we increase the charge density to $\eta_0 = 0.51$, we observe a transition to a NI* mode (dotted curve) with all the injected particles reaching the anode in the stationary regime. Further increasing η_0 from this point we note that the electromagnetic fields at the anode present a linear grow. This occurs because the number of electrons trapped in the gap region gradually decreases with increasing η_0. This occurs up to $\eta_0 = 2.21$ when there are no more trapped electrons and the stationary flow passes from the NI* to the NI mode (dotted-dashed curve). From this point on, the electromagnetic fields become decreasing functions of η_0 again. Finally, when the charge intensity reaches $\eta_0 = 3.14$, the electric field at the cathode vanishes [see Fig. 4(b)] and the flow becomes space charge limited. A virtual cathode emerges inside the gap and the less energetic electrons that were reaching the anode will be decelerated by the electric potential barrier and will return to the cathode. Hence, the flow goes from NI to PI again.

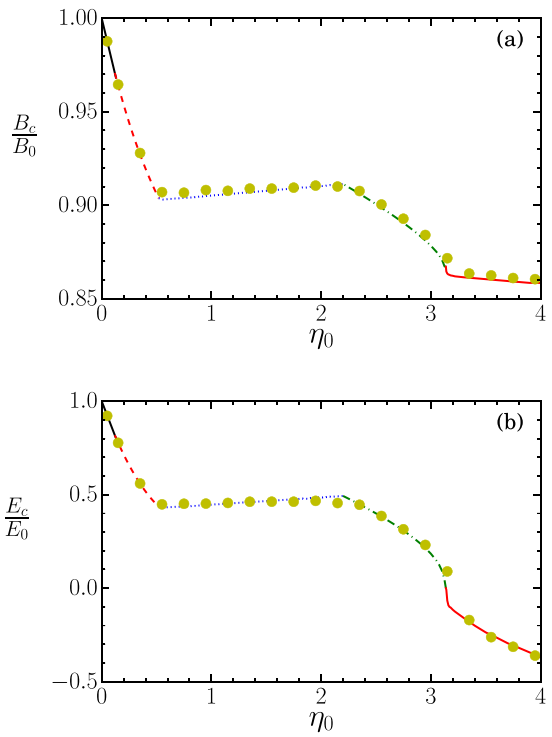

FIG. 4. Normalized magnetic (a) and electric (b) fields at the cathode as a function of the charge density η_0 for a fixed $T_0 = 0.006$. The curves correspond to the theoretical results: solid line refers to the MI mode, dotted line to the PI mode, dashed line to the NI* mode, and dashed-dotted line to the NI mode. The symbols are the results obtained from the $N-$ particle simulations. The remainder parameters are the same as those in Fig. 3(b).

It is worth noting that although the electric field is negative for $\eta_0 > 3.14$, we still find stationary solutions because of the finite temperature.[17] Moreover, increasing the normalized density even further will not lead to other stationary mode transitions, such that space charge limited cases are always PI modes.

V. NUMERICAL SIMULATIONS

In order to verify the results from the theory, we run N-particle self-consistent numerical simulations. In the simulations, electrons are emitted from the cathode at position $y = 0$ with an initial momentum determined by the waterbag distribution Eq. (6). The dynamics of each particle is derived from the Hamiltonian described in (4), resulting in

$$\frac{dy_i}{dt} = \frac{P_y^i}{\sqrt{m^2c^2 + e^2(A_x^i)^2 + (P_y^i)^2}}, \tag{13}$$

$$\frac{dP_y^i}{dt} = -\frac{ce^2 A_x^i B_z^i}{\sqrt{m^2c^2 + e^2(A_x^i)^2 + (P_y^i)^2}} - eE_y^i(y), \tag{14}$$

where $1 \le i \le N$ is the particle label and N is the total number of particles in the gap region. The electromagnetic fields are computed from Eqs. (2) and (3) using Green's function method.[26] When an electron reaches the anode or returns to the cathode, it is removed from the simulation. The simulations are initialized with an empty gap region ($N = 0$). As the time evolves, N starts to vary eventually reaching the stationary state. In the simulations presented here, the number of electrons in the gap region in the stationary state ranges from 7500 to 15 000, which was found to be large enough to give a proper description of the electron flow.

In Fig. 4, the circles correspond to the results obtained from the simulations for the normalized magnetic and electric field at the cathode once the flow becomes time independent. We note that there is a very good agreement between theoretical (curves) and simulational (circles) results.

For the parameters of Fig. 4, we noticed that the stationary flow suffers a series of mode transitions as the normalized charge density is increased from $\eta_0 = 0$. More specifically, these transitions are MI → PI → NI* → NI → PI as discussed above [or see Fig. 3(b)]. To perform a more detailed comparison between the theoretically predicted stationary state and the one obtained from the simulations, let us look at the phase space distributions obtained for each one of these modes. In Fig. 5(a), for $\eta_0 = 0.05$, the self-fields are *small* such that the flow is MI. The theoretical profile in this case is dictated by Eq. (9), which depends on $\pm P_y(y, P_{0max})$ that is represented by the solid curve in Fig. 5(a). We see that there is a perfect agreement between $\pm P_y(y, P_{0max})$ and the boundary of the particle distribution from the simulation. When $\eta_0 = 0.4$, the self-fields are more intense than in the previous case and now the more energetic particles reach the anode, as shown in Fig. 5(b). This characterizes the PI mode with uniform density theoretically described by Eq. (11). The curves $P_y(y, P_{0max})$ and $\pm P_y(y, P_{0lim})$ that describe this density are shown in the figure. While the particles contained between

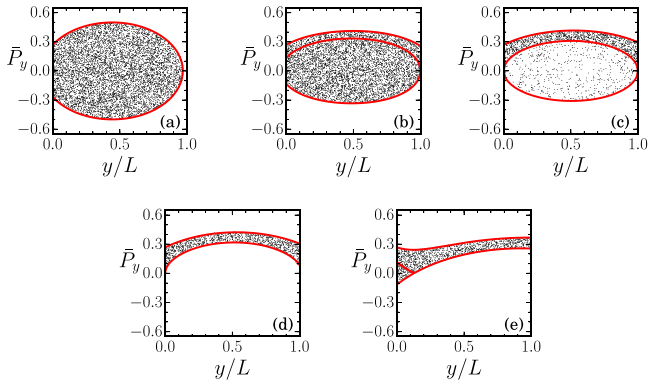

FIG. 5. Phase space plots of the stationary state for different values of the density parameter η_0. The dots correspond to the particle position in phase space obtained from simulations after the flow attained a stationary state. The solid curves show the proper distribution boundaries $[\pm P_y(y,0), \pm P_y(y, P_{0max}), \pm P_y(y, P_{0lim})]$ predicted by the theory for the corresponding stationary mode solution. Varying the charge density leads to transitions between different stationary modes: for $\eta_0 = 0.05$ (a) the flow is MI, for $\eta_0 = 0.40$ (b) the flow is PI, for $\eta_0 = 1.5$ (c) the flow is NI*, for $\eta_0 = 2.35$ (d) the flow is NI, and for $\eta_0 = 3.75$ (e) the flow returns to PI. The remainder parameters are the same as those in Fig. 4. $\bar{P}_y$ corresponds to the normalized momentum.

$P_y(y, P_{0lim})$ and $P_y(y, P_{0max})$ reach the anode, those contained between $\pm P_y(y, P_{0lim})$ return to the cathode. When $\eta_0 = 1.5$, Fig. 5(c), we see the appearance of two populations of particles with distinct densities in the phase space. Theoretically, this corresponds to the NI* mode described by the density of Eq. (12). The lower density population is formed by particles that were trapped inside the gap region before the stationary state was attained. They are distributed in the region between $\pm P_y(y, 0)$. Because their velocity vanishes at both the cathode and the anode, they can never leave the system. The higher density population corresponds to particles that are launched from the cathode after the formation of the stationary state. They all reach the anode and are distributed between $P_y(y, 0)$ and $P_y(y, P_{0max})$. For comparison, the curves $\pm P_y(y, 0)$ and $P_y(y, P_{0max})$ are shown in the figure. When $\eta_0 = 2.35$, Fig. 5(d), the lower density distribution of trapped particles of the previous case disappears and all the particles emitted from the cathode reach the anode with finite velocities. This characterizes the NI mode theoretically described by the density given in Eq. (10). All the particles are contained between the curves $P_y(y, 0)$ and $P_y(y, P_{0max})$ which are shown in the figure. Increasing even more the normalized density to $\eta_0 = 3.75$, Fig. 5(e), the space charge becomes high enough to create a virtual cathode in the gap and put the system in the space charge limited regime. The virtual cathode created by the self-electric field forces the particles back to the cathode. While the lower energy particles are not able to transpose this barrier and return to the cathode, the higher energy particles do reach the anode. This corresponds to a PI mode with a density theoretically described by Eq. (11). The curves $P_y(y, P_{0max})$ and $\pm P_y(y, P_{0lim})$ that describe this density are shown in the figure. It is worth to stress that the perfect agreement between the boundaries of the particles distribution obtained numerically and the corresponding theoretical curves $[\pm P_y(y, 0)$, $\pm P_y(y, P_{0max})$, etc.] for all the cases presented in Fig. 5 give

a strong support to the validity of the theoretical approach developed here to determine the stationary state.

VI. CONCLUSION

We have developed and analyzed a fully kinetic theory for the relativistic electron flow in a crossed-field device. The theory takes into account both self-electric and self-magnetic fields and allows determining the final stationary state achieved by the electrons in phase-space. We have identified a number of different possible stationary modes and described their characteristics. Particular attention was given to the study of how space charge and thermal effects affect the magnetic insulation when the external magnetic field exceeds the Hull cutoff field. In the nonrelativistic limit it was found that there is only a single transition from a MI to a PI mode as the injection temperature is increased. This transition is completely independent of the normalized electron density. On the other hand, in a moderate relativistic limit when the self-magnetic fields start to play a role, we found a much richer scenario in the parameter space. A series of stationary state mode transitions that go all the way from complete insulation (when no electrons reach the anode) to no insulation at all (when all the electrons reach the anode) occur as both injection temperature and charge density are varied. In particular, it was found that the transitions occur even at very low injection temperatures. Moreover, two different types of non-insulated stationary states were identified. While in the so called NI mode there is only a single population of electrons where all contribute to the cathode-anode current, in its variant NI^* there are two distinct electron populations: one that contributes to the cathode-anode current and a more tenuous one that stays trapped in the gap region, not contributing to the cathode-anode current. Despite the fact that the self-magnetic field plays a major role in the mode transitions in the relativistic case, we noticed that the net variations in the total magnetic field can be relatively small. For the particular case considered, we found that changes as small as 4% in the magnetic field at the cathode were sufficient to drive the onset of cathode-anode current. This shows how sensitive the system is to magnetic field variations and, therefore, how important a proper description of the self-magnetic field is. We have also run N-particle self-consistent simulations to verify the theoretical results. A very good agreement was found between the theory and the numerical results, which provides strong support to the validity of the theoretical approach developed here.

ACKNOWLEDGMENTS

This work was supported by CNPq, Brazil, and by the Air Force Office of Scientific Research (AFOSR), USA, under the Grant No. FA9550-16-1-0280. S.M. acknowledges support from Grant No. ANR-11-IDEX-0004-02 Plas@Par.

[1]D. M. Goebel and I. Katz, *Fundamentals of Electric Propulsion: Ion and Hall Thrusters* (John Wiley & Sons, Inc., Hoboken, NJ, 2008).
[2]S. Marini and R. Pakter, Phys. Plasmas **24**, 053507 (2017).
[3]R. K. Verma, S. Maurya, and V. V. P. Singh, J. Electromagn. Waves Appl. **32**, 113 (2018).
[4]A. S. Gilmour, *Klystrons, Traveling Wave Tubes, Magnetrons, Crossed-Field Amplifiers, and Gyrotrons* (Artech House, Norwood, MA, 2011).
[5]J. Andersson and A. Anders, Phys. Rev. Lett. **102**, 045003 (2009), and references therein.
[6]A. W. Hull, Phys. Rev. **18**, 31 (1921).
[7]C. D. Child, Phys. Rev. **32**, 492 (1911).
[8]I. Langmuir, Phys. Rev. **21**, 419 (1923).
[9]P. Zhang, Á. Valfells, L. K. Ang, J. W. Luginsland, and Y. Y. Lau, Appl. Phys. Rev. **4**, 011304 (2017), and references therein.
[10]Y. Y. Lau, P. J. Christenson, and D. Chernin, Phys. Fluids B **5**, 4486 (1993).
[11]T. Westermann, Nucl. Instrum. Methods Phys. Res. A **290**, 529 (1990).
[12]M. Lopez, Y. Y. Lau, J. W. Luginsland, D. W. Jordan, and R. M. Gilgenbach, Phys. Plasmas **10**, 4489 (2003).
[13]R. V. Lovelace and E. Ott, Phys. Fluids **17**, 1263 (1974).
[14]G. H. Goedecke, B. T. Davis, C. Chen, and C. V. Baker, Phys. Plasmas **12**, 113104 (2005).
[15]G. H. Goedecke, B. T. Davis, and C. Chen, Phys. Plasmas **13**, 083104 (2006).
[16]S. Marini, F. B. Rizzato, and R. Pakter, Phys. Plasmas **21**, 083111 (2014).
[17]S. Marini, F. B. Rizzato, and R. Pakter, Phys. Plasmas **23**, 033107 (2016).
[18]I. K. Baek, M. Sattorov, R. Bhattacharya, S. Kim, D. Hong, S. H. Min, and G. S. Park, IEEE Trans. Electron Devices **64**, 3413 (2017).
[19]S. Marini, F. B. Rizzato, and R. Pakter, in *Proceedings of IPAC, Richmond, VA* (2015), Paper No. MOPWA002.
[20]L. C. Martins, F. B. Rizzato, and R. Pakter, J. Appl. Phys. **106**, 043305 (2009).
[21]M. Reiser, *Theory and Design of Charged Particle Beams* (Wiley-Interscience, New York, 1994).
[22]W. A. Stygar, T. C. Wagoner, H. C. Ives, P. A. Corcoran, M. E. Cuneo, J. W. Douglas, T. L. Gilliland, M. G. Mazarakis, J. J. Ramirez, J. F. Seamen, D. B. Seidel, and R. B. Spielman, Phys. Rev. Spec. Top. Accel. Beams **9**, 090401 (2006).
[23]A. Antoniazzi, F. Califano, D. Fanelli, and S. Ruffo, Phys. Rev. Lett. **98**, 150602 (2007).
[24]Y. Levin, R. Pakter, F. B. Rizzato, T. N. Teles, and F. P. C. Benetti, Phys. Rep. **535**, 1 (2014).
[25]D. J. Kaup, Phys. Plasmas **11**, 3151 (2004).
[26]F. B. Rizzato, R. Pakter, and Y. Levin, Phys. Rev. E **80**, 021109 (2009).